Optimization for an Isoflux Pattern From a Multiring Microstrip Array via Least-Squares Regression

Seong-Yeop Jeong, Teak-Kyung Lee, *Member, IEEE*, and Jae-Wook Lee, *Member, IEEE*

***Abstract*—This letter presents a novel optimization via the theoretical modeling of an array geometry for isoflux patterns from a satellite antenna. The array has a multiring geometry capable of realizing the source distribution and ring radii similar to a sinc function shape. Additionally, the array uses the sequential changing of the phase excitations in order to favor circular polarization. By means of the cavity model, a synthesized electric field from the array antenna is formulated. For the desired isoflux pattern, the formulated electric field is analytically optimized via the least-squares regression iteration process. The results of the optimization show the approximately uniform electric-field illumination on the ground from a satellite antenna.**

***Index Terms*—Antenna arrays, circular polarization, isoflux patterns, optimization.**

I. Introduction

In SATELLITE applications, the efficient consumption of limited energy has always received significant attention. To save energy in satellite operations, the isoflux pattern, which enables uniform power illumination over wide area of the Earth's surface, has been investigated in numerous studies. Within these studies, helix, choke ring, horn, and crossed dipole antennas were employed [1]–[4]. To reduce satellite weights and launch costs, low-profile and lightweight planar array antennas have been actively studied for satellites orbiting at various altitudes [5]–[7].

In the literature, an isoflux pattern array was implemented in a Galileo navigation antenna in which the geometry was hexagonal for good rotational symmetry [5]. The isoflux pattern was realized via the excitations of the 180° phase difference between the inner and outer sections of the array. For antennas that did not rely as much on excitation devices, a multiring array was adopted [6]. The excitations and the positions of array elements were simultaneously optimized using an evolutionary optimization algorithm. In addition, an optimization for the excitations and positions of the elements was performed based on the sinc or Bessel function to generate a desired pattern [7].

The complexity and time consumption of the optimization procedure can be significantly reduced if the excitation optimizations are analytically performed for the fixed element positions. An iteration process with respect to the element positions can subsequently be performed in order to obtain the isoflux pattern. Given that the array geometry is likely to generate isoflux patterns, an analytical approach is more powerful.

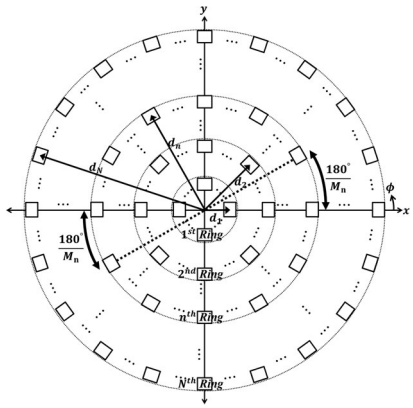

Fig. 1. Top view of general two-dimensional multiring array geometry on *x*–*y* plane.

This letter presents a multiring array designed to generate an isoflux pattern optimized for the uniform illumination on the ground from a satellite antenna. Least-squares regression [8] is employed as an analytical optimization tool for the excitations for the array elements. By means of the iteration process with respect to ring radii, the desired isoflux pattern is efficiently realized. The potential to design a satellite array antenna for use in medium Earth orbit (MEO) is, then, demonstrated with 20 elements. An isoflux pattern from the designed array antenna is visualized, and it provides an approximately uniform synthesized electric field on the ground.

II. Multiring Array for Isoflux Pattern

Using the Fourier transform relationship between the source distributions and far-field patterns, the isoflux pattern in the far-field region is obtained by manipulating electric current excitations on rectangular microstrip patches. To make it possible to radiate the isoflux pattern before the fitting optimization, the array geometry must be capable of realizing current excitations similar to a sinc function. One can see that the multiring array in Fig. 1 makes it possible to radiate isoflux patterns.

In Fig. 1, the geometry of the array is composed of N rings, and equal rectangular microstrip patches are used for all elements. In each ring, microstrip patches are concentrically arranged with equal angular intervals on the *x*–*y* plane. The patches in the nth ring have the same excitation, e_{n}. Hence, the excitation of patches in the array is expressed as an excitation vector, $\boldsymbol{e} = [e_1, e_2, \ldots, e_N]^T$. The radius from the origin to the center of patches in the $n\mathrm{th}$ ring is d_n. Thus, the radii of the rings for the array in Fig. 1 are indicated by a radius vector,

Manuscript received August 20, 2017; accepted September 14, 2017. Date of publication September 28, 2017; date of current version November 8, 2017. This work was supported by the Space Core Technology Development Program funded by the Ministry of Education, Science and Technology under Grant NRF-2017M1A3A3A02016484. *(Corresponding Author: Teak-Kyung Lee.)*

The authors are with the School of Electronics and Information Engineering, Korea Aerospace University, Goyang 10540, South Korea (e-mail: kotr7724@gmail.com; tklee@kau.ac.kr; jwlee1@kau.ac.kr).

Color versions of one or more of the figures in this letter are available online at http://ieeexplore.ieee.org.

Digital Object Identifier 10.1109/LAWP.2017.2757521

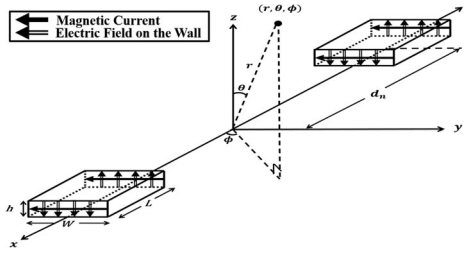

Fig. 2. Electric field and equivalent magnetic current on the side walls of two patches.

$\boldsymbol{d} = [d_1, d_2, \ldots, d_N]^T$. To find the best fit of isoflux patterns on the ground, it is of interest to see how the electric field from the array antenna is synthesized.

The patches in the ring are arranged symmetrically with respect to the origin, and the excitations on each pair of patches facing each other with the center of origin possess the same amplitude and phase. The angular intervals between the pairs in the ring are determined by considering both the patch size and the minimum distance between patches to be larger than 0.5λ. The number of pairs in the *n*th ring is assumed to be an even number and is denoted by M_n. Then, the pairs of patches in the nth ring are equally spaced by 180°/M_n in an angular direction, as indicated in Fig. 1. In terms of phase differences, because circular polarization is preferable in satellite communications, the excitation phase of the two patches of each pair in a ring is sequentially increased by 180°/M_n in the ϕ-direction. Because the number of pairs is even in every ring, a pair of patches always has another pair arranged in an orthogonal configuration, and the excitation phases of the two pairs differ by 90° to generate the circular polarization.

Considering the aforementioned arrangement, the formulation of the synthesized electric field from the satellite antenna is initiated by analyzing the far-field radiation from a pair of patches. Fig. 2 shows a pair of patches in the *n*th ring, which is symmetrically placed along the *x*-axis. The distances from the origin to the center of the patches are d_n.

In the array antenna, all of the microstrip patches have the same dimensions. From the cavity model for the fundamental mode [9], via the Equivalent Principle with the electric field on the side walls of microstrip patches, the equivalent magnetic currents are distributed as in Fig. 2 ($L > W \gg h$). The electric field intensity in the far-field region radiated by these equivalent magnetic currents on a pair of patches is

$$\boldsymbol{E}^{\text{pair}}(r,\theta,\phi) = e_n \left[E^{\text{pair}}_{\theta n}(r,\theta,\phi)\,\hat{\boldsymbol{\theta}} + E^{\text{pair}}_{\phi n}(r,\theta,\phi)\,\hat{\boldsymbol{\varphi}} \right] \quad (1)$$

where e_n is the magnitude of excitation for the patches in the nth ring, and

$$E^{\text{pair}}_{\theta n} \approx \frac{j8k_0 e^{-jk_\circ r}}{\pi r}\cos\phi \left[\cos(k_x d_n)\cos\left(\frac{k_x L}{2}\right)\right] \times \frac{\sin(k_y W/2)}{k_y}$$

$$E^{\text{pair}}_{\phi n} \approx \frac{j8k_0 e^{-jk_\circ r}}{\pi r}\cos\theta\sin\phi \left[\cos(k_x d_n)\cos\left(\frac{k_x L}{2}\right)\right] \times \frac{\sin(k_y W/2)}{k_y}$$

$$k_x = k_0\sin\theta\cos\phi,\ k_y = k_0\sin\theta\sin\phi.$$

Here k_0 is the free-space wavenumber, and h is assumed to be very small compared to the patch size.

Considering the aforementioned angular intervals and phase differences in each ring, the synthesized electric field from the entire array of patches in Fig. 1 can be expressed in the far-field region by

$$\begin{aligned}\boldsymbol{E}^{\text{total}}(r,\theta,\phi) &= \sum_{n=1}^{N} e_n \sum_{m=0}^{M_n-1}\left[e^{j\frac{\pi m}{M_n}}\boldsymbol{E}^{\text{pair}}\left(r,\theta,\phi-\frac{\pi m}{M_n}\right)\right] \\ &= \sum_{n=1}^{N} e_n\left[E^{\text{total}}_{\theta n}(r,\theta,\phi)\,\hat{\boldsymbol{\theta}} + E^{\text{total}}_{\phi n}(r,\theta,\phi)\,\hat{\boldsymbol{\varphi}}\right].\end{aligned} \quad (2)$$

In (2), it can be seen that the electric field intensity is synthesized by adjusting two coefficient sets of excitation vector $\boldsymbol{e}$ and radius vector $\boldsymbol{d}$.

III. Optimization of Excitations and Radii

The optimization procedure is carried out to obtain a uniform magnitude of electric-field intensity on the desired illumination region with the low side-lobe level. Radius vector $\boldsymbol{d}$ and excitation vector $\boldsymbol{e}$ are iteratively optimized until the simulated radiation pattern satisfies the mask pattern. In each iteration, the excitation vector is optimized for a given radius vector. If the error exceeds the limit in an iteration, a new radius vector $\boldsymbol{d}$ is applied to the optimization process. It is of interest to learn that how to determine the value of $\boldsymbol{e}$ that causes the magnitude of the electric field intensity on the ground to become a constant value, C, within the coverage angle as

$$\left|\boldsymbol{E}^{\text{ground}}\right| \approx C \quad 0<\theta<\Theta;\ 0<\phi<2\pi \quad (3)$$

where Θ indicates a half of the coverage angle.

Considering the geometry of the Earth and the altitude of the satellite, the distance from the satellite to the Earth's surface, r_g, is determined for θ and ϕ. From (2), the electric field intensity radiating from the array on the ground is

$$\boldsymbol{E}^{\text{ground}}(\theta,\phi) = \sum_{n=1}^{N} e_n\left[E^{g}_{\theta n}(\theta,\phi)\,\hat{\boldsymbol{\theta}} + E^{g}_{\phi n}(\theta,\phi)\,\hat{\boldsymbol{\varphi}}\right]. \quad (4)$$

An array antenna with an isoflux pattern is designed by optimizing the excitation vector, $\boldsymbol{e}$, in (4) to satisfy (3). This excitation vector is optimized using least-square regression iteratively. The errors derived from (3) are calculated at sample points within the coverage angle. The overall squared error, SE, is given by

$$\text{SE} = \sum_{q=1}^{Q}\sum_{p=1}^{P}\left[C - \left|\sum_{n=1}^{N} e_n\left[E^{g}_{\theta n}\left(\theta_p,\phi_q\right)\hat{\boldsymbol{\theta}} + E^{g}_{\phi n}\left(\theta_p,\phi_q\right)\hat{\boldsymbol{\varphi}}\right]\right|\right]^2 \quad (5)$$

where P and Q are the number of sampling points in the θ and ϕ directions, respectively. When $0<\theta<\Theta$ and $0<\phi<2\pi$, the sampling points are uniformly spaced in both directions.

When employing least-squares regression, SE must be partially differentiable with respect to $\boldsymbol{e}$. For the isoflux pattern, it is assumed that the excitation takes a sinc function shape, ensuring that the excitation of the patches in first ring, e_1, is much

stronger compared to that of the other rings. Thus, SE can be approximated as

$$\mathrm{SE} \approx \sum_{q=1}^{Q}\sum_{p=1}^{P}\left[C - \sum_{n=1}^{N} e_n \left| E_{\theta n}^{g}\left(\theta_p, \phi_q\right)\hat{\boldsymbol{\theta}} + E_{\phi n}^{g}\left(\theta_p, \phi_q\right)\hat{\boldsymbol{\varphi}}\right|\right]^2. \tag{6}$$

The excitations $e_1, e_2, \ldots, e_N$ for the patches providing the minimum SE are obtained by solving

$$\left[\frac{\partial}{\partial e_1}\mathrm{SE} \quad \frac{\partial}{\partial e_2}\mathrm{SE} \quad \cdots \quad \frac{\partial}{\partial e_N}\mathrm{SE}\right]^T = 0. \tag{7}$$

Through the inverse of the matrix from (7), the optimal excitation vector for a given radius vector is given by

$$\begin{bmatrix} e_1 \\ e_2 \\ \vdots \\ e_N \end{bmatrix} = \begin{bmatrix} \sum_{q=1}^{Q}\sum_{p=1}^{P} {E_1}^2 & \sum_{q=1}^{Q}\sum_{p=1}^{P} E_1E_2 & \cdots & \sum_{q=1}^{Q}\sum_{p=1}^{P} E_1E_N \\ \sum_{q=1}^{Q}\sum_{p=1}^{P} E_1E_2 & \sum_{q=1}^{Q}\sum_{p=1}^{P} {E_2}^2 & \cdots & \sum_{q=1}^{Q}\sum_{p=1}^{P} E_2E_N \\ \vdots & \vdots & \ddots & \vdots \\ \sum_{q=1}^{Q}\sum_{p=1}^{P} E_1E_N & \sum_{q=1}^{Q}\sum_{p=1}^{P} E_2E_N & \cdots & \sum_{q=1}^{Q}\sum_{p=1}^{P} {E_N}^2 \end{bmatrix}^{-1} \times \begin{bmatrix} C\sum_{q=1}^{Q}\sum_{p=1}^{P} E_1 \\ C\sum_{q=1}^{Q}\sum_{p=1}^{P} E_2 \\ \vdots \\ C\sum_{q=1}^{Q}\sum_{p=1}^{P} E_N \end{bmatrix} \tag{8}$$

where

$$E_n = \left(\left|E_{\theta n}^{g}\left(\theta_p, \phi_q\right)\right|^2 + \left|E_{\phi n}^{g}\left(\theta_p, \phi_q\right)\right|^2\right)^{1/2}.$$

The optimized excitation vector $\boldsymbol{e}$ in (8) causes the magnitude of the electric field intensity on the ground to be maximally uniform at C.

The least-squares regression indicated by dotted line in Fig. 3 is a portion of whole iteration process. The parameter sets are the initial radius vector, $\boldsymbol{d}_i = [d_{1i}, d_{2i}, \ldots, d_{Ni}]^T$, and the increment vector of the ring's radii, $\boldsymbol{\alpha} = [\alpha_1, \alpha_2, \ldots, \alpha_N]^T$. Starting from the initial radius vector, in each iteration, the radius vector, which is updated by the increment vector, is applied to the least-squares regression. This iteration is carried out until the simulated pattern satisfies the mask pattern. The increment value of the first ring is the smallest for the fine optimization because the influence of the first ring over radiation pattern is stronger than that of the other rings. With the process in Fig. 3, the desired solutions for $\boldsymbol{e}$ and $\boldsymbol{d}$ are efficiently found.

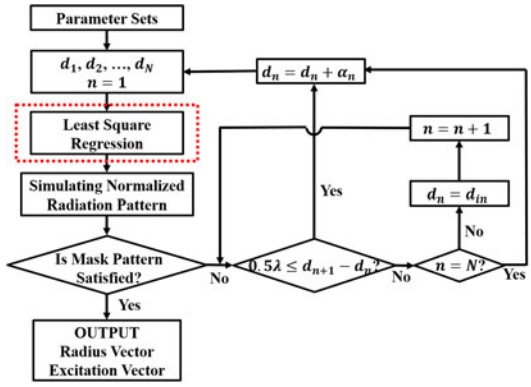

Fig. 3. Flowchart of iteration process.

TABLE I
PARAMETER SET ($C = 9\times10^{-6}$)

	Initial Radius Vector (cm)	Increment Vector of Radii (cm)
First Ring	13	0.5
Second Ring	24	2

TABLE II
ITERATIVE PROCESS RESULT

	Excitation Vector	Radius Vector (cm)
First Ring	5.8789×10^4	13
Second Ring	-1.1209×10^4	40

IV. DESIGN OF AN MEO SATELLITE ANTENNA

To verify the optimization, a satellite antenna with an isoflux pattern for use in MEO is designed to demonstrate the applicability of the approach. It is assumed that the antenna requires a coverage angle of around 20°, and the boresight of the antenna is directed toward the center of the Earth. Additionally, the cross-section of the Earth is assumed to be a perfect circle. The altitude of the satellite is 23 616 km from the ground. The operating frequency is 1.5 GHz, and the dielectric constant of the substrate is 2.2. The dimensions of the patch are $L = 6.7$, $W = 5.6$, and $h = 0.157$ cm. There are two rings, and the numbers of pairs are $M_1 = 4$ and $M_2 = 6$ for the first and second rings, respectively. To ensure that the minimum distance between patches exceeds 0.5λ, radii d_1 and d_2 need to be larger than 13 and 23 cm, respectively. The parameter sets are in Table I.

From these parameter sets, the iteration process is conducted using MATLAB. The consuming time for the optimization is 344 s and the number of iterations is 137. Table II gives the results for the excitation vector and radius vector from the iteration process, and these results are used to calculate the magnitude of the electric field intensity on the ground in Fig. 4. One can see that, within $\theta < 10°$, the maximum error percentage between the magnitude of electric field on the ground and the C value is around 5.56% at $\theta \approx 10°$ in Fig. 4. From an approximately uniform magnitude of the electric field on the ground, a satisfactory isoflux radiation pattern is observed in Fig. 5(a) with a coverage angle of over 20°. Our calculation in solid curve is compared with the EM simulation by CST Studio in which

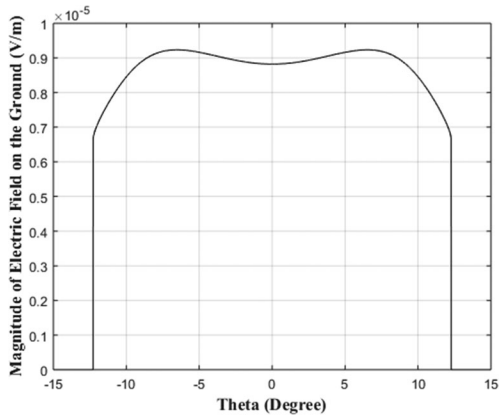

Fig. 4. Magnitude of electric field on the ground.

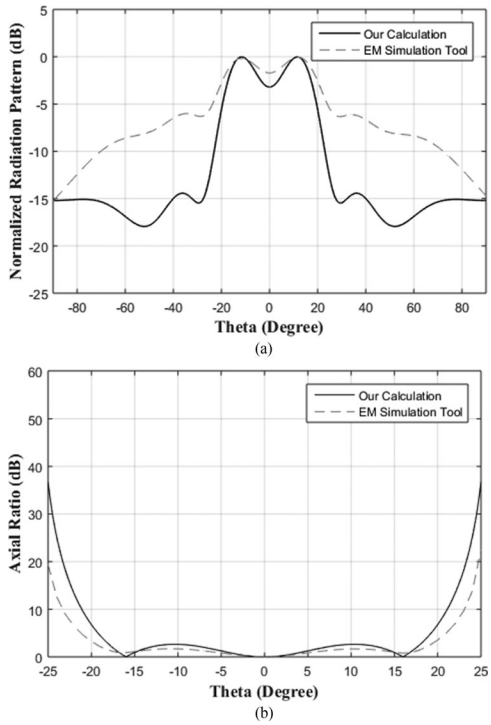

Fig. 5. (a) Normalized radiation pattern. (b) Axial ratio of the designed array.

the probe feeding method was taken. The two patterns show the same coverage angle and about 1 dB maximum difference. The comparison in the main lobe validates that the suggested method is suitable in optimizing an isoflux pattern. The difference in the range of $\theta > 10^{\circ}$ is interpreted due to the unideal surface current distributions on patches in the EM simulation. The calculated axial ratio is nearly close to the EM simulation, and both are less than 2.7 dB in the range of $\theta < 10^{\circ}$ in Fig. 5(b).

As expected, the intensity of e_1 is around five times stronger than e_2 in Table II. In addition, the ring radii d_1 and d_2 correspond to the mid-points between the origin and the sequential nulls in the sinc function. This implies that the array geometry can easily follow a sinc function shape via the excitation vector and radius vector, and the optimization is reasonable. Moreover, the array has a relatively low number of elements (20 patches) and small diameter (86.7 cm) compared to [5]. In Fig. 6, the pairs in the first and second rings are arranged with equal

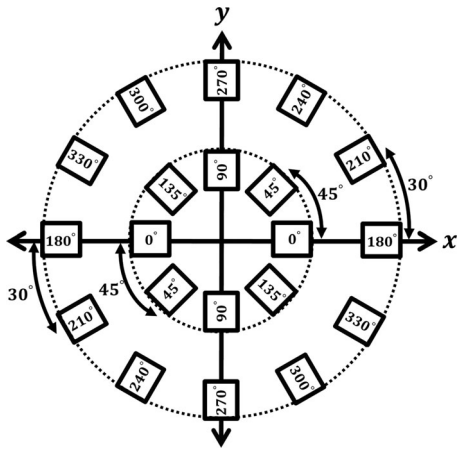

Fig. 6. Top-view of satellite antenna array with 20 elements.

angular intervals of 45° and 30°, respectively. The excitation phases denoted on the patches in Fig. 6 are sequentially increased by 45° and 30° for first and second rings, respectively.

V. Conclusion

An optimization procedure for the design of an array antenna with an isoflux pattern has been presented and verified for multiring geometry. Least-squares regression was employed as an iteration algorithm to determine the optimal excitaton vector and radius vector. From the results of the iteration process, it was demonstrated that it was possible to design an MEO satellite antenna with an approximately uniform electric field on the ground within the coverage angle. Additionally, the designed array showed a relatively small number of elements and diameter. Through innovative research on feeding networks, it would be possible to implement the proposed antenna. In addition, the procedure could be exploited in the synthesis of other radiation patterns with array antennas.

Reference

[1] J. Fouany *et al.*, "Circularly polarized isoflux compact X band antenna for nano-satellites applications," in *Proc. 12th Eur. Conf. Radar*, 2015, pp. 381–384.

[2] J. Wettergren, P. Dimming, J. F. Johansson, and M. Ohgren, "A high gain X-band isoflux helix antenna," in *Proc. 10th Eur. Conf. Antennas Propag.*, 2016.

[3] E. Martini, F. Caminita, M. Faenzi, G. Minatti, and S. Maci, "New antennas for space applications," in *Proc. URSI Int. Symp. Electromagn. Theory*, 2016, pp. 103–106.

[4] E. C. Choi, J. W. Lee, T. K. Lee, and W. K. Lee, "Equivalent model analysis of modified satellite antenna for isoflux pattern generation," *J. Electromagn. Eng. Sci.*, vol. 14, pp. 278–283, Sep. 2014.

[5] A. Montesano *et al.*, "Galileo system navigation antenna for global positioning," in *Proc. 2nd Eur. Conf. Antennas Propag.*, 2007.

[6] M. Ibarra, A. G. Andrade, M. A. Panduro, and A. L. Mendez, "Design of antenna arrays for isoflux radiation in satellite systems" in *Proc. 33th Int. Conf. IEEE Perform. Comput. Commun.*, 2014.

[7] K. Xu, H. Li, Z. Zhu, J. Huangfu, C. Li, and L. Ran, "Versatile beam forming with concentric excitations based on multiple weighted sinc or Bessel function distribution" *IEEE Trans. Antennas Propag.*, vol. 61, pp. 4082–4090, Aug. 2013.

[8] A. Gilat and V. Subramaniam, "Curve fitting and interpolation," in *Numerical Methods: An Introduction With Applications Using MATLAB*, 2nd ed. Hoboken, NJ, USA: Wiley, 2011.

[9] C. A. Balanis, "Microstrip Antennas," in *Antenna Theory: Analysis and Design*, 3rd ed. New York, NY, USA: Wiley, 2005.